World Academy of Science, Engineering and Technology
International Journal of Mechanical and Mechatronics Engineering
Vol:14, No:7, 2020

Dynamic Behaviors of a Floating Bridge with Mooring Lines under Wind and Wave Excitations

Chungkuk Jin, Moohyun Kim, Woo Chul Chung

***Abstract*—**This paper presents global performance and dynamic behaviors of a discrete-pontoon-type floating bridge with mooring lines in time domain under wind and wave excitations. The structure is designed for long-distance and deep-water crossing and consists of the girder, columns, pontoons, and mooring lines. Their functionality and behaviors are investigated by using elastic-floater/mooring fully-coupled dynamic simulation computer program. Dynamic wind, first- and second-order wave forces, and current loads are considered as environmental loads. Girder's dynamic responses and mooring tensions are analyzed under different analysis methods and environmental conditions. Girder's lateral responses are highly influenced by the second-order wave and wind loads while the first-order wave load mainly influences its vertical responses.

***Keywords*—**Floating bridge, elastic dynamic response, coupled dynamics, mooring line, pontoon, wave/wind excitation, resonance, second-order effect.

I. Introduction

A floating bridge is designed for the deep-water with soft bed and long-distance crossings. The floating bridge is a proven technology because there are many such bridges in the world, including the USA, Norway, Canada, Japan, Guyana, and Australia. Most of the previous floating bridges are for cars, bikes, and people while trains are also considered in some floating-bridge designs.

The oldest and most popular design is based on continuous rectangular pontoons as a backbone with secondary discrete stability-supporting pontoons to reduce roll motions. Although this design has been proven by long years of service, it is not considered as an optimal design, at least to the author's point of view in that, (1) the continuous rectangular pontoons are non-parent and tend to block all wave and current forces, so structurally (including mooring lines) extremely burdened, (2) its buoyancy is too much, so excessive amount of ballast needs to be used, which is also very expensive, (3) mooring tension can be extremely burdened by the change of sea level by tidal variation, and (4) no space for ship's navigation. In this regard, the floating bridges with discretize pontoons have been mainly proposed by Norwegian Public Roads Administration (NPRA) to cross fjords in Norway [1].

Several studies were conducted to investigate the dynamic and structural behaviors of floating bridges. Cheng et al. [2] evaluated the performance of a curved floating bridge under wave excitations. Cheng et al. [3] also investigated the effects of the second-order drift load on the curved floating bridge. Fu et al. [4] compared the results of their numerical model with experimental results under moving loads. Fredriksen et al. [5] performed the pontoon optimization of a side-anchored floating bridge. Wei et al. [6] evaluated the dynamic responses of a curved floating bridge under inhomogeneous waves.

In this study, dynamic responses of a straight floating bridge with mooring lines are investigated by using the fully-coupled dynamic simulation program in the time domain. This floating bridge is similar to the design suggested to cross Bjørnafjorden by NPRA. For modeling simplicity, we only model the girder, pontoons, columns, and mooring lines, whereas a cable-stayed bridge in the left end is not considered. Wave loads and hydrostatic and hydrodynamic coefficients for pontoons are obtained from the frequency-domain computations through a 3D diffraction/radiation panel program. The time-domain analysis is successively performed by OrcaFlex [7]. The first- and second-order wave drift, wind, and current loads are considered.

II. Design and Methodology

A. Design

Fig. 1 shows the entire design of a floating bridge with mooring lines, and Tables I-III summarize the corresponding design parameters. The 3800-m-long straight floating bridge is considered, which is similar to the floating bridge designed for Bjørnafjorden. However, the cable-stayed bridge in the left end is not modeled for simplicity. 17 pontoons are uniformly spaced with an interval of 203 m. Pontoons are made of lightweight concrete, and their height and draft are 14.5 and 10.5 m, respectively. A total of 18 mooring lines are installed to keep the position. Each mooring group consists of six mooring lines, and three mooring groups are connected to the pontoon #3, #9, and #15, respectively. The mooring lines consist of R5 chain at the top, steel-wire at the middle, and R4 chain at the bottom. On top of each pontoon, a circular column, which is made of steel with a diameter of 10 m, is positioned to connect pontoons with the girder. The girder, which is made of steel and concrete, is connected to the top of the columns. At the locations of girder contacting with columns, the supporting material (S1 type in Table III) is added. Abutments are placed at both ends of the girder so that fixed boundary conditions can be made. For simplicity, water depth is fixed to be 500 m.

Chungkuk Jin is with the Department of Ocean Engineering, Texas A&M University, College Station, TX, 77843 USA (corresponding author, e-mail: kenjin0519@gmail.com)

Moohyun Kim and Woo Chul Chung are with the Department of Ocean Engineering, Texas A&M University, College Station, TX, 77843 USA (e-mail: m-kim3@tamu.edu, kracus83@gmail.com)

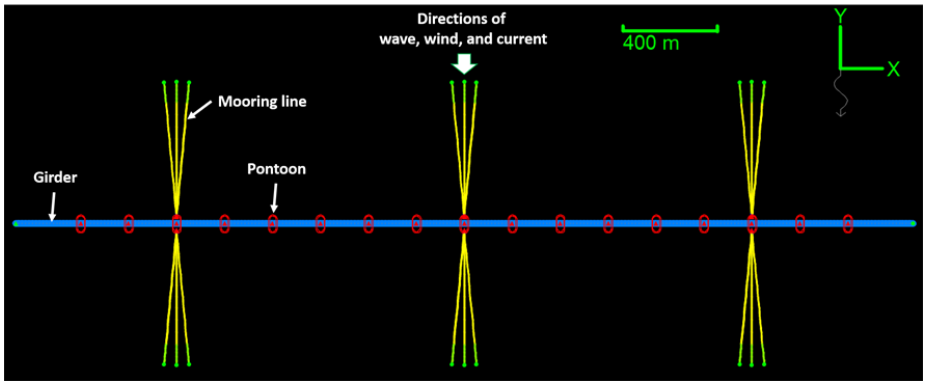

Fig. 1 Numerical modeling of the floating bridge with mooring lines

TABLE I
DESIGN PARAMETERS: PONTOON

Item	Value	Unit
Length	28	m
Width	68	m
Height	14.5	M
Mass	11,300	t
Roll inertia	4,900,000	$t{\cdot}m^2$
Pitch inertia	1,360,000	$t{\cdot}m^2$
Yaw inertia	5,700,000	$t{\cdot}m^2$
Center of gravity	(0, 0, -4.2)	m
Center of buoyancy	(0, 0, -5.4)	m
Heave stiffness	17.5	MN/m
Roll water plane stiffness	5,700	MNm/rad
Pitch water plane stiffness	1,000	MNm/rad

Note that in the Tables, E is young's modulus, G is shear modulus, A is the cross-sectional area, I_Y and I_Z are the second moments of area about the weak and strong axes, respectively, while I_X is the torsional second moment of area.

TABLE II
DESIGN PARAMETERS: MOORING LINE

Item	Value			Unit
	R5 Chain	Wire	R4 Chain	
Length	20	641	100	m
Nominal diameter	0.175	0.175	0.175	m
Mass	783	203	685	kg/m
EA	2.6×10^9	1.6×10^9	2.4×10^9	N

TABLE III
DESIGN PARAMETERS: GIRDER AND COLUMN

Item	Value			Unit
	Girder S1	Girder F1	Column	
Mass	24,900	19,700	14,300	kg/m
EA	4.4×10^{11}	3.1×10^{11}	3.2×10^{11}	N
EI_Y	3.6×10^{12}	2.6×10^{12}	4.0×10^{12}	Nm^2
EI_Z	3.7×10^{13}	2.5×10^{13}	4.0×10^{12}	Nm^2
GI_X	4.4×10^{12}	3.1×10^{12}	3.1×10^{12}	Nm^2

B. Methodology

Fig. 2 shows the modeling methodology for the floating bridge. OrcaFlex is used for entire modeling and time-domain simulations. Each pontoon is modeled by a 6-degree-of-freedom (6DOF) rigid body while a line model is used for modeling other components. The connection of components is completed by using linear and rotational springs. To connect the girder and columns, the entire girder is divided into 17 girder sections, and their connections are made by introducing a dummy 6DOF rigid body. The dummy rigid body is only utilized for connection purposes and does not affect the overall dynamics with negligible mass and no external loads. Through sufficiently large values of translational and rotational stiffness, the rigid connection can be made among girder sections, columns, and pontoons. Similarly, the adoption of sufficiently large values of translational stiffness and negligible values of rotational stiffness can model the hinged connection between pontoons and mooring lines. Authors have presented a detailed methodology and its validation in the previous study with regard to the submerged floating tunnels [8], [9].

The general equation of motion for the entire structure can be expressed as:

$$\mathbf{M}\ddot{\boldsymbol{\xi}} + \mathbf{C}\dot{\boldsymbol{\xi}} + \mathbf{K}\boldsymbol{\xi} = \mathbf{F} \tag{1}$$

where $\mathbf{M}$, $\mathbf{C}$, and $\mathbf{K}$ are the mass, damping, stiffness matrices while $\boldsymbol{\xi}$ and $\mathbf{F}$ are the displacement and external load vectors, respectively. Overdot represents the time derivative of a variable.

Frequency- and time-domain analyses are required for floating bodies with water contact, which can be pontoons in this case. In the frequency domain, the boundary value problem for the linear velocity potential is solved, and the corresponding hydrodynamic coefficients and wave loads are obtained at each frequency. The 3D diffraction/radiation program is used to solve for these coefficients and wave loads, which are transferred to the time-domain simulation program to solve the time-domain equation of motion. The time-domain equation of motion for floating bodies can be written as:

$$[\mathbf{M} + \mathbf{M}_\mathbf{A}(\infty)]\ddot{\boldsymbol{\zeta}} + (\mathbf{K}_\mathbf{H} + \mathbf{K}_\mathbf{S})\boldsymbol{\zeta} = \mathbf{F}_{\mathbf{W1}} + \mathbf{F}_{\mathbf{W2}} + \mathbf{F}_\mathbf{C} + \mathbf{F}_\mathbf{N} \tag{2}$$

where $\mathbf{M}_\mathbf{A}(\infty)$ is the added mass matrix at the infinite frequency, $\mathbf{K}_\mathbf{H}$ and $\mathbf{K}_\mathbf{S}$ are the hydrostatic restoring and spring stiffness matrices while $\mathbf{F}_{\mathbf{W1}}$, $\mathbf{F}_{\mathbf{W2}}$, $\mathbf{F}_\mathbf{C}$, and $\mathbf{F}_\mathbf{N}$ are the first-order wave load, second-order wave load, radiation-damping load, and viscous drag load vectors, respectively. The added mass matrix at the infinite frequency and radiation-damping load can be expressed as:

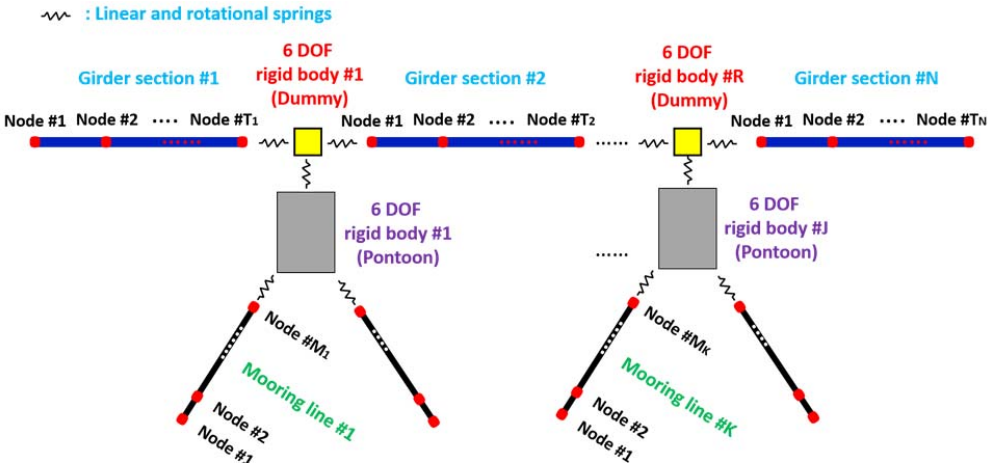

Fig. 2 Modeling methodology of a floating bridge

$$\mathbf{M}_{\mathbf{A}}(\infty)=\mathbf{M}_{\mathbf{A}}(\omega)+\int_0^{\infty}\mathbf{R}(t)\frac{\sin(\omega t)}{\omega}dt$$
$$\mathbf{F}_{\mathbf{C}}=-\int_0^{t}\mathbf{R}(\tau)\dot{\zeta}(t-\tau)d\tau \quad (3)$$
$$\mathbf{R}(t)=\frac{2}{\pi}\int_0^{\infty}\mathbf{C}_{\mathbf{R}}(\omega)\cos(\omega t)\,d\omega$$

The radiation damping coefficient $\mathbf{C}_{\mathbf{R}}$ is caused by energy dissipation associated with wave making by floater motions. $\mathbf{R}$ in the above convolution integral is called the retardation function and can be obtained from the Fourier cosine transform of $\mathbf{C}_{\mathbf{R}}$.

In random waves, the first- and second-order wave loads can be expressed by using the two-term Volterra series expansion as [10]-[12]:

$$F_{W1}=\mathrm{Re}\sum_{j=1}^{N}A_j f_j e^{-i\omega_j t}$$
$$F_{W2}=\mathrm{Re}\sum_{j=1}^{N}\sum_{k=1}^{N}\begin{bmatrix}A_j A_k^{*} f_{jk}^{-}(\omega_j,\omega_k)e^{-i(\omega_j-\omega_k)t}\\ +A_j A_k^{*} f_{jk}^{+}(\omega_j,\omega_k)e^{-i(\omega_j+\omega_k)t}\end{bmatrix} \quad (4)$$

where A is complex wave amplitude, N is the number of wave components, and f_j and $f_{jk}^{\pm}$ are the linear (LTF) and quadratic force transfer functions (QTF), i.e., respective wave forces due to unit-amplitude monochromatic and bichromatic incident waves. In this study, the second-order sum-frequency wave loads are not considered because its role is negligible. Newman's approximation is utilized to estimate the second-order difference-frequency (or slowly-varying) wave drift loads. The viscous drag load, $\mathbf{F}_{\mathbf{N}}$, can be obtained by using the Morison equation for a slender moving object. The Morison equation can be written as:

$$\mathbf{F}_{\mathbf{M}}=-C_A\rho V_E\ddot{\boldsymbol{\xi}}+C_M\rho V_E\dot{\mathbf{V}}+\frac{1}{2}C_d\rho A_E\left|\mathbf{V}-\dot{\boldsymbol{\xi}}\right|\left(\mathbf{V}-\dot{\boldsymbol{\xi}}\right)$$
$$\mathbf{F}_{\mathbf{N}}=\frac{1}{2}C_D\rho A_E\left|\mathbf{V}-\dot{\boldsymbol{\xi}}\right|\left(\mathbf{V}-\dot{\boldsymbol{\xi}}\right) \quad (5)$$

where C_A, C_M, and C_D are the added mass, inertia, and drag coefficient, respectively, ρ is the density of surrounding fluid, $\mathbf{V}$ is the velocity of fluid while V_E and A_E are displaced volume and frontal area of the object. In case of (2), the first term of (5), $\mathbf{F}_{\mathbf{M}}$, is equivalent to the added mass term $\mathbf{M}_{\mathbf{A}}$, and the second term of (5) is equivalent to wave-induced inertia force by $\mathbf{F}_{\mathbf{WI}}$. So, only viscous drag force $\mathbf{F}_{\mathbf{N}}$ is added on the right-hand side of (2). In case of mooring-line dynamics, the total Morison force $\mathbf{F}_{\mathbf{M}}$ is directly used.

The girder, columns, and mooring lines are modeled by the lumped-mass-method-based elastic line (or elastic Euler beam) model, in which a line is divided into nodes and segments. Mass, buoyancy, drag, and other properties are all lumped at each node while neighboring nodes are connected by massless springs representing axial, bending, and torsional properties. For these objects, equivalent loads on the elements are calculated and applied in the nodes. Similarly, equivalent axial, bending, and torsional stiffness values are also utilized. Elastic behaviors can be represented by dividing a line into several nodes and elements. Wave loads on mooring lines are estimated by using the Morison equation. For the girder and columns, since they are exposed to air only, the viscous drag load in the Morison equation is solely utilized for wind force calculations. Also, in the girder, the static traffic load in the vertical direction is applied.

III. Environmental Condition

Wave, wind, and current are considered as the input environmental condition. Fig. 3 shows the wave and wind spectra. For waves, typical 100-year storm and ocean swell waves in Norway Fjord are considered. Significant wave heights of the storm and swell waves are 3.0 m and 0.4 m while their peak periods are 6 (1.05 rad/s) and 12 (0.52 rad/s) seconds. Jonswap wave spectrum is adopted to generate random waves by superposing 100 regular waves. Enhancement parameters are set to be 5.0 and 1.0 for storm and ocean swell waves, respectively. 1-year dynamic wind is considered with a mean wind speed of 22.9 m/s at a height of 10 m and the random wind velocities were generated by using the API wind spectrum and

superposing 1000 sinusoidal components. Constant current is considered with a current velocity of 0.7 m/s. The direction of environmental loads is 270°, as illustrated in Fig. 1. The simulation time for each case is 3,600 s.

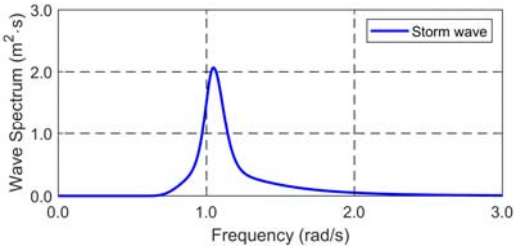

(a)

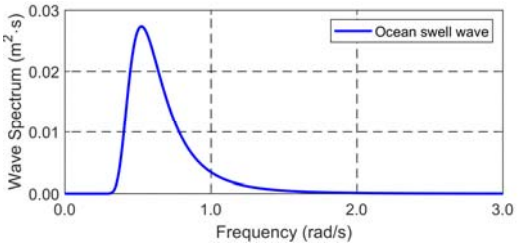

(b)

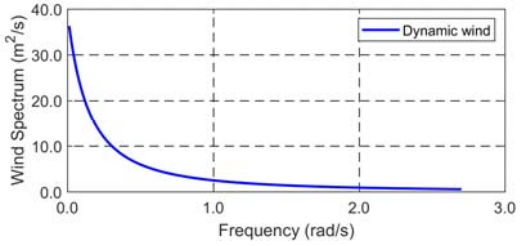

(c)

Fig. 3 Spectra of storm (a) and ocean swell (b) waves and wind (c)

IV. Results and Discussions

The girder's dynamic responses, mooring tensions, and their time series and spectra are systematically analyzed in different environmental loads to evaluate the importance of each load. In specific, envelopes of the standard deviations and the motion spectra are presented along the girder's longitudinal direction while time histories are only presented for the middle section. Note that the lowest natural frequencies in the lateral and vertical directions are 0.10 rad/s and 0.57 rad/s. It means that the lowest natural frequency for the lateral motion is lower than wave-frequency range, whereas that of vertical motion is in the range of incident-wave frequencies. We consider three loading combinations, i.e., Case 1 to Case 3 (Case 1: first-order wave load only, Case 2: first- and second-order wave loads, Case3: first-order wave load as well as wind and current loads)

Figs. 4 and 5 show the envelopes of standard deviation (STD) of the girder's lateral and vertical responses under different loading conditions. For lateral responses, large motions are observed in the central location, for which both second-order wave loads and wind loads play a crucial role. For vertical responses, motion STDs are mostly induced by the first-order wave loading, and the role of second-order wave force and wind loads is relatively minor.

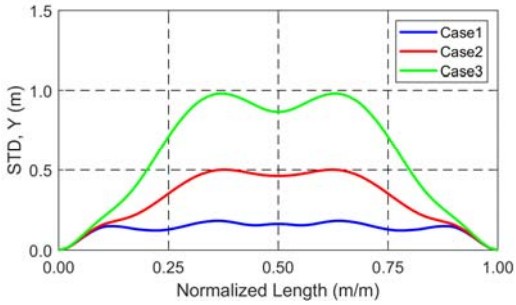

Fig. 4 STD of the girder's lateral responses under different loads

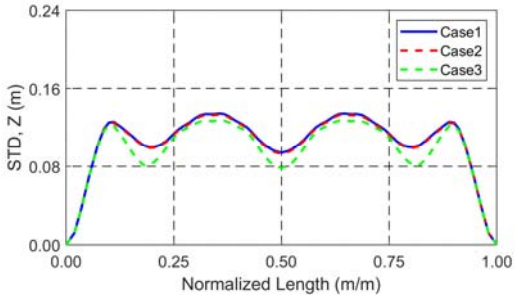

Fig. 5 STD of the girder's vertical responses under different loads

Fig. 6 shows the STDs of mooring tensions at the respective lines under different loads. Mooring tensions tend to follow the trends of girder's lateral and vertical responses. The wind loads significantly increase the dynamic tension magnitudes especially at the taut side of the middle section, i.e., mooring #10, #11, and #12. The maximum mooring tension is 6,160 kN observed at the mooring line #10 in Case 3, which is still below the MBL (Minimum breaking load). Note that the MBL of the wire mooring is 24,300 kN, and its safety factor is 1.67.

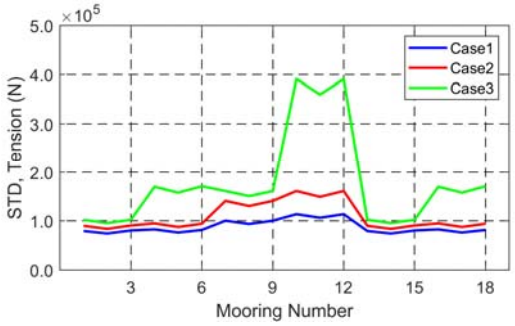

Fig. 6 STDs of mooring tensions under different loads

Fig. 7 shows the time histories of the girder's lateral and vertical responses at the middle section under three different loading conditions. The lateral responses show that low-frequency motions are dominant as the second-order wave forces and wind loads are additionally considered. The energy of these loads is in the lower frequency range than that of the first-order wave load. Then, resonance occurs at the lowest

natural frequency of the lateral motion and it significantly increases the maximum response magnitudes. On the other hand, the second-order wave forces and wind loads have little influence on vertical responses.

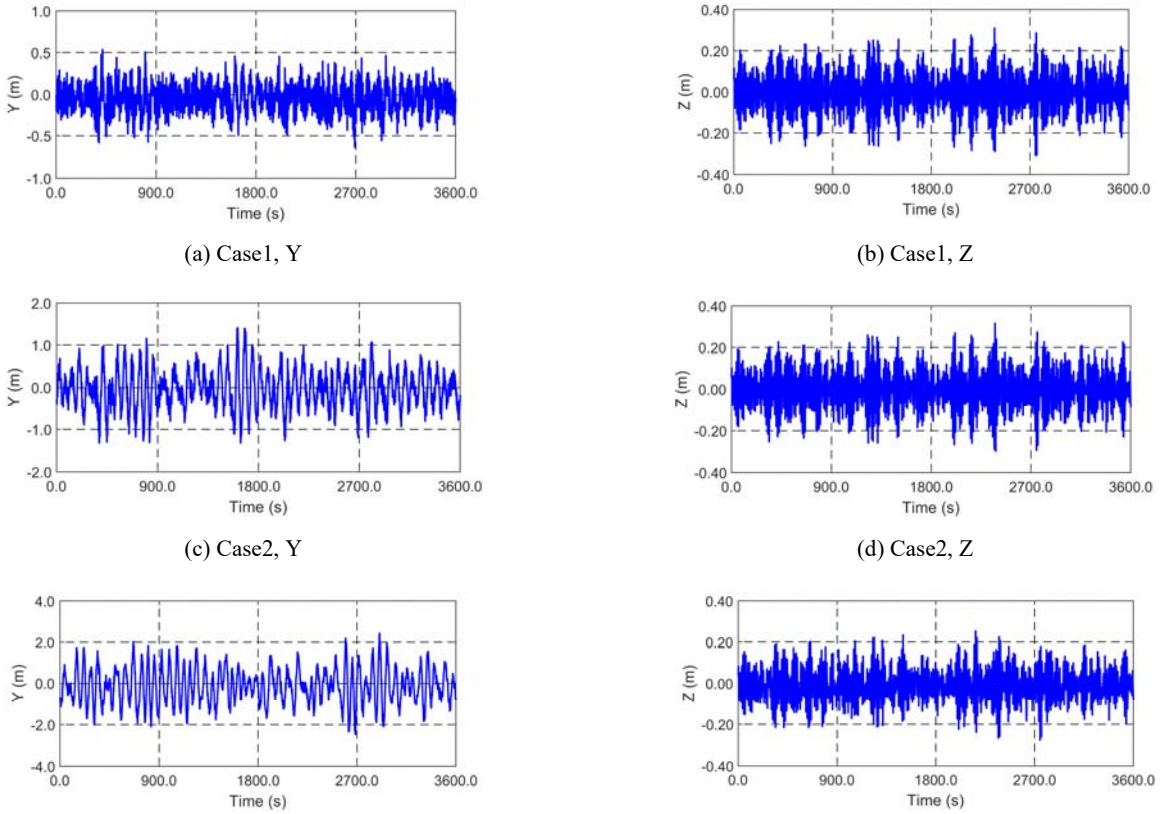

(a) Case1, Y (b) Case1, Z

(c) Case2, Y (d) Case2, Z

(e) Case3, Y (f) Case3, Z

Fig. 7 Time histories of girder's lateral and vertical responses under different loading conditions

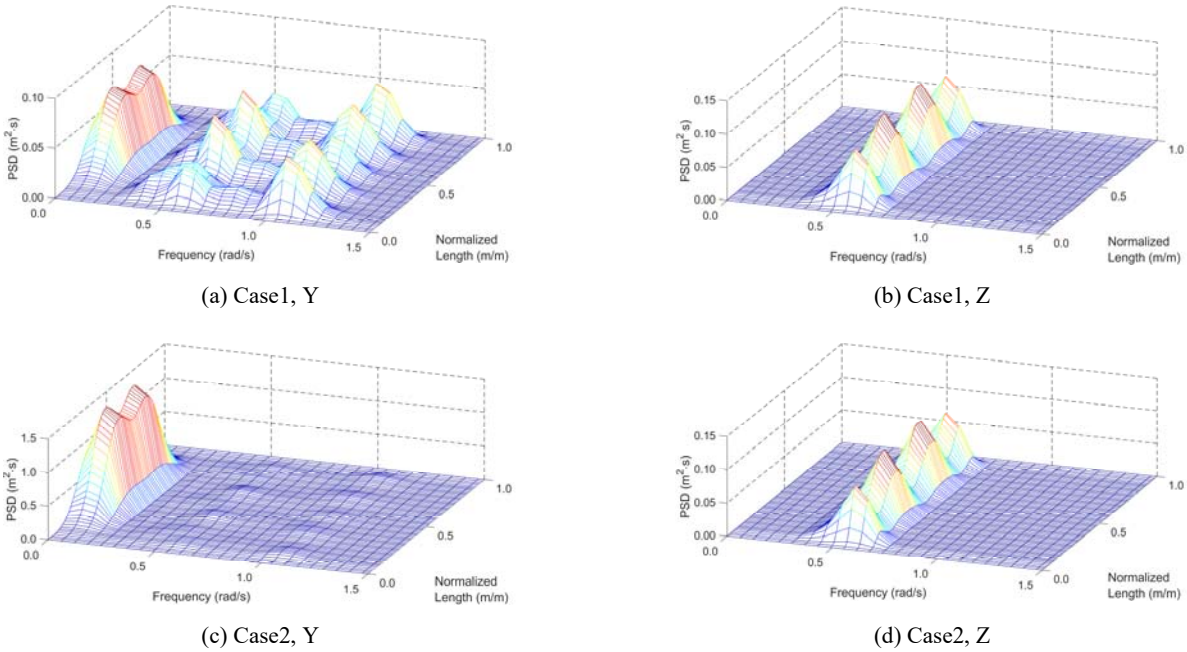

(a) Case1, Y (b) Case1, Z

(c) Case2, Y (d) Case2, Z

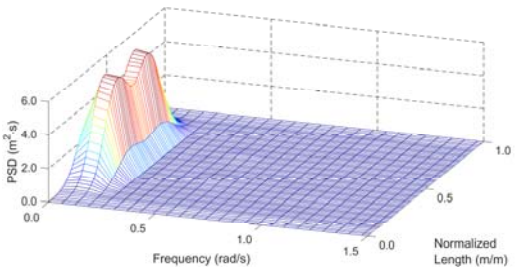

(e) Case3, Y

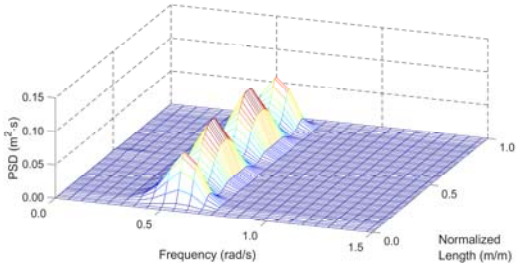

(f) Case3, Z

Fig. 8 Spectra of girder's lateral and vertical responses along the girder's longitudinal direction under different loading conditions

Fig. 8 shows the corresponding spectra of the girder's lateral and vertical responses under three different loading conditions as a function of frequency and the girder's longitudinal position. When the first-order wave load is solely considered, there are three minor peaks in the lateral responses. The lowest peak is at the lowest natural frequency in the lateral direction around 0.10 rad/s while second and third peaks are located at the frequency of ocean swell and storm waves, respectively. The small wave excitation near 0.10 rad/s is originated from the nonlinear Morison drag force. As the second-order wave and wind loads are additionally considered, resonance-induced responses around 0.10 rad/s are enlarged and become dominant while the relative importance of wave-frequency responses at the storm and swell frequencies becomes small. The fluctuation of peak magnitudes in the longitudinal direction is due to the influence of mooring positions. Next, let us examine the spectra of vertical responses. It is clear that vertical responses, having the lowest natural frequency at 0.57 rad/s, are little influenced by the low-frequency excitations from the second-order difference-frequency wave forces and slowly-varying wind loads. Also, the direction of wind loads is mainly in the lateral direction, which has no noticeable effect on vertical responses. Since the lowest natural frequency in the vertical direction is close to the frequencies of ocean swell waves, we see dominant peaks there. Again, the variation of peak magnitudes in the longitudinal direction is due to the influence of mooring positions.

V. Conclusion

Dynamic behaviors of a 3800-m-long discrete-pontoon-type floating bridge with mooring lines are investigated in time-domain by using elastic-floater/mooring fully-coupled dynamic simulation computer program. Dynamic wind, first- and second-order wave forces, and current loads are considered as environmental loadings. We checked the girder's dynamic responses and mooring tensions, which turn out to be acceptable for design and functionality. The girder's lateral responses are mainly influenced by the second-order difference-frequency wave and slowly-varying wind loads since they are close to the lowest lateral natural frequency. On the other hand, the first-order wave load plays a major role in its vertical responses.

Acknowledgment

This work was supported by Hyundai Engineering & Construction. This work was also supported by the National Research Foundation of Korea (NRF) grant funded by the Korea government (MSIT) (No. 2017R1A5A1014883).

References

[1] M.E. Eidem, "Overview of floating bridge projects in Norway." ASME 2017 36th International Conference on Ocean, Offshore and Arctic Engineering, OMAE2017-62714, 2017.
[2] Z. Cheng, Z. Gao, T. Moan, "Wave load effect analysis of a floating bridge in a fjord considering inhomogeneous wave conditions," Engineering Structures, 163, 197-214, 2018.
[3] Z. Cheng, Z. Gao, T. Moan, "Hydrodynamic load modeling and analysis of a floating bridge in homogeneous wave conditions," Marine Structures, 59, 122-141, 2018.
[4] S. Fu, W. Cui, X. Chen, C. Wang, "Hydroelastic analysis of a nonlinearly connected floating bridge subjected to moving loads," Marine Structures, 18, 85-107, 2005.
[5] A.G. Fredriksen, M.F. Heiervang, P.N. Larsen, P.G. Sandnes, B. Sørby, B. Bonnemaire, et al., "Hydrodynamical Aspects of Pontoon Optimization for a Side-Anchored Floating Bridge," Journal of Offshore Mechanics and Arctic Engineering, 141, 031603, 2019.
[6] W. Wei, S. Fu, T. Moan, C. Song, S. Deng, H. Lie, "A Time-domain method for hydroelasticity of a curved floating bridge in inhomogeneous waves," Journal of Offshore Mechanics and Arctic Engineering, 141, 014501-1, 2019.
[7] Orcina. OrcaFlex Manual, 2018.
[8] C. Jin, M.-H. Kim, "Time-domain hydro-elastic analysis of a SFT (submerged floating tunnel) with mooring lines under extreme wave and seismic excitations," Applied Sciences, 8, 2386, 2018.
[9] C. Jin, M.-H. Kim, "Tunnel-mooring-train coupled dynamic analysis for submerged floating tunnel under wave excitations," Applied Ocean Research, 94, 102008, 2020.
[10] M.H. Kim, D.K.P. Yue, "Sum-and difference-frequency wave loads on a body in unidirectional Gaussian seas," Journal of Ship Research, 35, 127-140, 1991.
[11] M.-H. Kim, D.K.P. Yue, "The complete second-order diffraction solution for an axisymmetric body Part 2. Bichromatic incident waves and body motions," Journal of Fluid Mechanics, 211, 557-593, 1990.
[12] M.-H. Kim, "Difference-frequency wave loads on a large body in multi-directional waves," Applied ocean research, 14, 353-370, 1992.